Relative intensities of 3p-3s transitions in neonlike Ar IX

N. Preissing, D. O. Campos, and H.-J. Kunze
Institut für Experimentalphysik V, Ruhr-Universität, 44780 Bochum, Federal Republic of Germany

A. L. Osterheld and R. S. Walling
Lawrence Livermore National Laboratory, P.O. Box 808, Livermore, California 94550

(Received 19 March 1993)

Argon was added in small amounts to θ-pinch discharges in hydrogen and deuterium, and the relative intensities of all $3p \rightarrow 3s$ transitions of neonlike argon were measured at the peak of the Ar IX concentration. At this time recombination was small since the ion was in an ionizing regime; effective excitation of the $3p$ levels was essentially due to direct collisional excitation from the ground state and cascading contributions after excitation to higher levels. The relative intensities are compared with theoretical calculations, which employed various collisional and radiative transition rates given in the literature. Very good overall agreement is obtained with a collisional-radiative model which includes all levels up to $n=5$.

PACS number(s): 52.70.La, 34.80.Kw, 42.55.Vc

Soft-x-ray lasers advanced remarkably during the last couple of years, which became obvious again at the recent international conference on x-ray lasers [1]. A general introduction to the field of x-ray lasers and a rather comprehensive elucidation of the problems as well as a review of the achievements until about 1989 may be found in the monograph by Elton [2].

A variety of pumping schemes to produce population inversion are pursued, but collisional excitation of neonlike and nickel-like ions and three-body recombination of hydrogenlike and lithiumlike ions in laser-produced plasmas have been most successful so far. Despite the progress, some basic physics issues of x-ray lasers remain poorly understood. One example has become known as the "$J=0-1$ anomaly" in neonlike ions, and the most recent publications do not resolve the problem [3,4]. Theoretical modeling predicts the highest gain on the $J=0$ to $J=1$ transition among all $3p \rightarrow 3s$ transitions of neonlike ions. However, the first report [5] of lasing in neonlike selenium was surprising in the relative absence of large gain on this transition, while lasing on two other $J=2$ to $J=1$ transitions was relatively stronger. The puzzle became even greater as other neonlike ions showed similar behavior but some did not [2,4]. Possible explanations are discussed by Elton [2].

The first idea that crosses one's mind is to question the reliability of the atomic physics that enters the kinetic modeling of the population densities. Doschek, Feldman, and Bhatia [6] studied the respective transitions in neonlike Fe XVII and compared the relative line intensities derived from spectra of solar flares with theoretical ones based on a simple collisional excitation model. Measured and theoretical intensities agreed to within less than a factor of 2 for all but one $J=2$ to $J=1$ line. The critical $J=0$ to $J=1$ transition was weaker by about a factor of 1.4, which was almost within observational error.

Motivating these solar studies were earlier experiments by Elton *et al.* [7,8], where the relative intensities in Cl VIII and Ar IX were measured. The observations were made on a hydrogen θ-pinch plasma with admixtures of freon (for chlorine) or argon. The electron density was 2.5×10^{16} cm^{-3} and the electron temperature was $kT_e=65$ eV. In units of the excitation energy $E(3p)$ of the $3p$ levels this corresponds to a ratio of $u=kT_e/E(3p)=0.24$ in the case of Ar IX. The authors compared the intensities with theoretical predictions and concluded that all major lines agree within 30%. Hence, no significant $n=3$ population irregularities appear, which could explain the anomalies in the higher-density laser experiments.

We now report similar experiments on Ar IX carried out on a larger θ-pinch device. The density is approximately the same, but the electron temperature is much higher, giving $u=0.74$ and 0.89.

The experimental setup has been used previously to study collisional excitation of multiply ionized atoms (e.g., Ref. [9]). At present the energy in the main bank is 100 kJ at a charging voltage of 35 kV. The quarter period is 5.75 μs, and the current is crowbarred at the current maximum. An initial low-reversed magnetic bias field of 0.06 T leads to the formation of a stable plasma column, which is destroyed by a $m=2$ rotational instability after about 10 μs. The θ-pinch coil is 61 cm long with an inner diameter of 21 cm. For these investigations a discharge tube with inner diameter of 15 cm was used.

Electron density and electron temperature were determined by Thomson scattering as a function of time and at several radial positions in the midplane of the coil. Two gas fillings were used, namely 19 mTorr hydrogen and 19 mTorr deuterium, both with 1% argon added. Figure 1 shows density and temperature averaged over the radius as a function of time for the hydrogen plasma.

For the spectroscopic measurements a 1-m normal-incidence vacuum ultraviolet monochromator was aligned to view the plasma axially. A 2400 grooves/mm grating was installed in order to resolve the closely

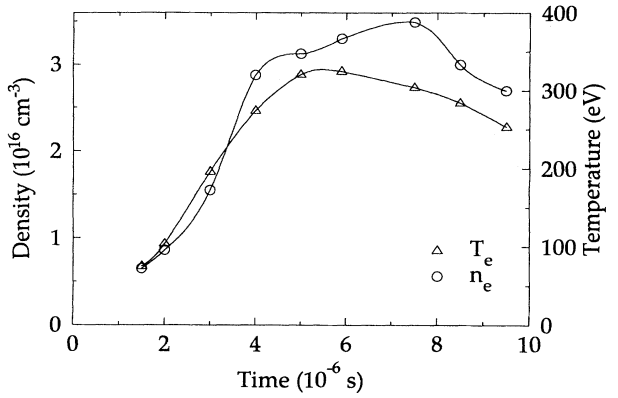

FIG. 1. Electron density and temperature averaged over the radius as function of time for the discharge in 19-mTorr hydrogen with 1% argon added.

spaced lines of the $\Delta n=0$ transitions, and a p-terphenyl scintillator and a photomultiplier at the exit slit allowed the time-resolved observation of the line emission. The relative spectral sensitivity of the complete system was obtained *in situ*, employing the branching-ratio method. Following Elton *et al.* [8], we spanned the wavelength range from 477 Å to 740 Å using a line pair each of O V and O VI. The estimated error was approximately ±15%.

After the initial compression of the plasma in the pinch coil, the electron temperature of the plasma column was already high and further increased rapidly until it leveled off. Because of finite ionization times, the state of ionization lagged far behind that of equilibrium for the respective electron temperature, and the argon ions went successively through the ionization stages until recombination began to become important. This behavior was confirmed by observing one or two lines from each ion of Ar VI to Ar XI. At $t=6$ μs after initiation of the discharge—Ar XI intensities peaked at $t=5.5$ μs—the influence of recombination became obvious. Ar IX had its peak at $t=3$ μs and hence could be considered to be in a truly ionizing regime in the plasma. Its line emission was studied at its peak, and at this time the concentration of the Ar X ion still was low, i.e., less than 30% of the Ar IX density. This is of great importance for the analysis of the line emission, because it assures that recombination from Ar X indeed is negligible. The line emission thus is governed by collisional excitation from the ground state; naturally, cascading after excitation to higher levels is included if important, and with increasing electron density collisional mixing between excited states may also have to be accounted for.

Tables I and II show the experimental results for the two discharge conditions in hydrogen and deuterium. The first column of each table gives the 15 $3p\rightarrow 3s$ transitions of Ar IX in LS notation, the second column contains their wavelengths. Transitions found to lase prominently in laser-produced plasmas are designated by A–F, following Refs. [2], [7], and [8]. The relative spectral radiances L_{expt} of all transitions as measured at their maximum are shown in the third column. They are normalized to the strong $^1D_2\rightarrow{}^3P_2$ transition at 642.34 Å; in this way uncertainties of the plasma length and of the argon concentration cancel.

For comparison with theoretical predictions, steady-state population densities n_i of the upper levels (i) were calculated. They were obtained as solutions of the coupled set of equations, which account for the population of the levels by collisional and radiative transitions within Ar IX,

$$\sum_{\substack{k,i\\k<i}} n_k n_e X_{ki} + \sum_{\substack{k,i\\k>i}} n_k (n_e X_{ki} + A_{ki}) - n_i \sum_{\substack{i,j\\i>j}} (n_e X_{ij} + A_{ij}) = 0 \,. \quad (1)$$

The spectral radiance L_{ij} of each $3p\rightarrow 3s$ transition was

TABLE I. Relative spectral radiance of the $2s^22p^53p\rightarrow 2s^22p^53s$ transitions of Ar IX in the hydrogen discharge. $n_e=1.7\times10^{16}$ cm^{-3} and $kT_e=200$ eV.

Transition	λ(Å)	L_{expt}	$\frac{L_{\text{expt}}}{L_{\text{Bha}}}$	$\frac{L_{\text{expt}}}{L_{\text{Zha}}}$	$\frac{L_{\text{expt}}}{L_{\text{Moh}}}$	L_{theor}	$\frac{L_{\text{expt}}}{L_{\text{theor}}}$
(A) $^1S_0\rightarrow{}^1P_1$	468.80	1.60	0.51	0.54	0.95	1.619	0.99
$^3P_1\rightarrow{}^3P_2$	589.41	0.11	1.00	1.10	1.10	0.149	0.74
$^3P_1\rightarrow{}^3P_0$	659.80	0.23	0.96	1.10	1.10	0.232	0.99
$^3P_1\rightarrow{}^1P_1$	692.60	0.27	1.07	1.17	1.23	0.250	1.08
(F) $^3P_0\rightarrow{}^3P_1$	628.76	0.06	1.00	1.00	2.00	0.068	0.88
$^1D_2\rightarrow{}^3P_2$	642.34	1.00	1.00	1.00	1.00	1.000	1.00
(B) $^1D_2\rightarrow{}^3P_1$	670.74	0.51	0.94	0.94	0.94	0.554	0.92
$^1P_1\rightarrow{}^3P_0$	691.20	0.26	1.04	1.13	0.84	0.259	1.00
$^3D_2\rightarrow{}^3P_2$	692.69	0.53	0.78	0.82	0.91	0.612	0.87
(E) $^3D_2\rightarrow{}^3P_1$	725.82	0.54	0.73	0.76	0.84	0.684	0.79
(D) $^3D_1\rightarrow{}^3P_1$	696.48	0.46	1.24	1.39	1.48	0.354	1.30
(C) $^3P_2\rightarrow{}^1P_1$	697.67	0.48	0.80	0.96	1.17	0.492	0.98
$^3D_3\rightarrow{}^3P_2$	697.59	2.86	0.81	0.84	0.89	3.381	0.85
$^1P_1\rightarrow{}^1P_1$	727.45	0.17	0.90	0.94	0.71	0.205	0.83
$^3S_1\rightarrow{}^3P_1$	860.59	0.17	0.81	0.81	0.77	0.172	0.99

TABLE II. Relative spectral radiance of the $2s^22p^53p \rightarrow 2s^22p^53s$ transitions of Ar IX in the deuterium discharge. $n_e = 1.4 \times 10^{16}$ cm^{-3} and $kT_e = 240$ eV.

Transition	λ(Å)	L_{expt}	$\frac{L_{\text{expt}}}{L_{\text{Bha}}}$	$\frac{L_{\text{expt}}}{L_{\text{Zha}}}$	$\frac{L_{\text{expt}}}{L_{\text{Moh}}}$	L_{theor}	$\frac{L_{\text{expt}}}{L_{\text{theor}}}$
(*A*) $^1S_0 \rightarrow {}^1P_1$	468.80	1.48	0.47	0.50	0.88	1.654	0.89
$^3P_1 \rightarrow {}^3P_2$	589.41	0.10	0.91	0.91	1.00	0.147	0.68
$^3P_1 \rightarrow {}^3P_0$	659.80	0.25	1.04	1.14	1.19	0.229	1.09
$^3P_1 \rightarrow {}^1P_1$	692.60	0.26	1.04	1.13	1.18	0.247	1.05
(*F*) $^3P_0 \rightarrow {}^3P_1$	628.76	0.08	1.60	1.33	2.67	0.067	1.19
$^1D_2 \rightarrow {}^3P_2$	642.34	1.00	1.00	1.00	1.00	1.00	1.00
(*B*) $^1D_2 \rightarrow {}^3P_1$	670.74	0.60	1.11	1.11	1.11	0.554	1.08
$^1P_1 \rightarrow {}^3P_0$	691.20	0.25	1.00	1.09	0.81	0.256	0.98
$^3D_2 \rightarrow {}^3P_2$	692.69	0.78	1.15	1.20	1.32	0.610	1.28
(*E*) $^3D_2 \rightarrow {}^3P_1$	725.82	0.85	1.15	1.20	1.33	0.682	1.25
(*D*) $^3P_1 \rightarrow {}^3P_1$	696.48	0.38	1.06	1.12	1.23	0.349	1.09
(*C*) $^3P_2 \rightarrow {}^1P_1$	697.67	0.31	0.56	0.62	0.76	0.496	0.63
$^3D_3 \rightarrow {}^3P_2$	697.59	2.50	0.70	0.73	0.78	3.361	0.74
$^1P_1 \rightarrow {}^1P_1$	727.45	0.20	1.05	1.11	0.83	0.203	0.99
$^3S_1 \rightarrow {}^3P_1$	860.59	0.23	1.05	1.05	1.05	0.173	1.33

then calculated from

$$L_{ij} = \frac{h\nu_{ij}}{4\pi} A_{ij} n_i l_p \ , \tag{2}$$

where l_p was the plasma length.

Our first calculations were based on radiative-transition probabilities A_{ki} and collisional rate coefficients X_{ki} as given by Bhatia, Feldman, and Seely [10] and Zhang *et al.* [11]. Thirty-six levels were considered; the configurations included $2s^22p^6$, $2s^22p^53s$, $2s^22p^53p$, $2s^22p^53d$, $2s^22p^54s$, $2s^12p^63p$, $2s^22p^54d$, and $2s^12p^64p$. The theoretical spectral radiances L were again normalized to the $^1D_2 \rightarrow {}^3P_2$ transition, and the fourth column gives the ratio of experimental radiance L_{expt} and theoretical radiance L_{Bha} obtained with the data of Bhatia, Feldman, and Seely [10]. If we exclude the "*A*" transition, the agreement between theory and experiment is surprisingly good for all transitions at both discharge conditions, the standard deviation from the mean being 15% and 23%, respectively. The *A* transition on the other hand, which shows the "$J = 0 - 1$ *anomaly*," is indeed weaker by a factor of 2 than theoretically expected.

A similar result is shown in the fifth column $L_{\text{expt}}/L_{\text{Zha}}$, obtained from calculations employing the theoretical rates of Zhang *et al.* [11]; the experimental "*A*" transition again is too weak by a factor of 2, whereas all the others deviate from the mean by 18% in both cases. When the collisional rates of Mohan are used [12] (column six $L_{\text{expt}}/L_{\text{Moh}}$), the radiances of the *A*, *B*, and *C* lasing lines agree with the theoretical values, the experimental *F* lasing line now being too strong. Because of this line, the overall agreement between theory and experiment is worse, the standard deviation of $L_{\text{expt}}/L_{\text{Moh}}$ from the mean being 31% and 41%, respectively. Our experimental result for the *A* line differs from that of Elton *et al.* [7], who found agreement with the data of Bhatia, Feldman, and Seely [10]. Their measurements were done, however, at a temperature that was lower than ours by a factor of 3.

We finally extended the collisional-radiative model up to $n = 5$, i.e., it consisted of a total of 157 levels. Wave functions, spontaneous rates, and direct excitation rates were calculated, including all states in the $2s^22p^6$ ground state and the excited configurations

$$2s^22p^5(3s, 3p, 3d, 4s, 4p, 4f, 5s, 5p, 5d, 5f, 5g) \ ,$$

$$2s^12p^6(3s, 3p, 3d, 4s, 4p, 4d, 4f, 5s, 5p, 5d, 5f, 5g) \ .$$

The atomic data were calculated using the HULLAC (Hebrew-University–Lawrence-Livermore Atomic Code) package developed at Hebrew University and LLNL. The wave functions, energy levels, and radiative-transition rates were calculated in the relativistic, multiconfiguration parametric potential model [13,14]. The direct-excitation cross sections between all states in the model were computed using a relativistic, distorted-wave method described by Bar-Shalom, Klapisch, and Oreg [15]. These cross sections go into a fitting procedure for the temperature-dependent excitation rate coefficients. The principle of detailed balance gives the corresponding deexcitation rate coefficients. The atomic data are similar to those used to model neonlike-selenium x-ray lasers [16]. In addition to these direct rates we included a set of indirect excitation rate coefficients from the $2s^22p^6$ ground state to all states in the $2s^22p^53s$ and $2s^22p^53p$ configurations by scaling the resonance excitation rates given in Ref. [17].

The results are given in the last two columns of Tables I and II for both discharge conditions. The seventh column displays the relative radiances L_{theor} and the column $L_{\text{expt}}/L_{\text{theor}}$ again the ratio of experimental and theoretical values. The overall agreement is surprisingly good, the *A* transition included. The standard deviation from the mean of all $L_{\text{expt}}/L_{\text{theor}}$ values is 15% for the hydrogen discharge and 21% for the discharge in deuterium. The experimental results thus confirm the best avail-

able calculations.

There still remains the puzzle of different relative gain of the A, B, and C lines in various gain experiments. An analysis of the population channels may offer an explanation. Figure 2 displays a partial energy-level diagram. The widths of the arrows indicate the relative strengths of the respective collisional excitation channels. For simplicity, the total excitation to the 12 $3d$ levels is represented by one arrow. The crux is the cascading contributions to the $3p$ levels and the temperature dependence of the excitation rates to the $3p$ and the $3d$ levels, the first being a monopole excitation and the second dipole excitation. Thus, with increasing temperature the dipole excitation and hence the cascading contributions become relatively stronger. The other crucial point is the negligibly smaller $3d\,^1P_1 \rightarrow 3p\,^1S_0$ cascading contribution because of the very strong decay of the $3d\,^1P_1$ level to the ground state; consequently, the $3p\,^1S_0$ level of the A laser line is populated essentially only by collisions from the ground state, in contrast to the upper levels of the other lasing lines where collisional excitation and cascading contribute by about equal amounts. As a result, the population densities of the upper levels display a different dependence on the temperature. Furthermore, any collisional mixing between the $3d$ levels at high electron densities will also affect the cascading contributions and hence the B and C laser lines. This suggests that a poorly known electron temperature and density can lead to deviating gain predictions for the various experiments.

It is certainly extremely difficult to determine with sufficient precision the time evolution of density and temperature of laser-produced plasmas, which are in a very transient state. In most cases, all plasma parameters were derived from time-integrated observations. However, in order to bring the discrepancy to a close, it is imperative to measure the electron temperature and density as function of time, and to model the kinetics of the excited levels with the best available atomic data.

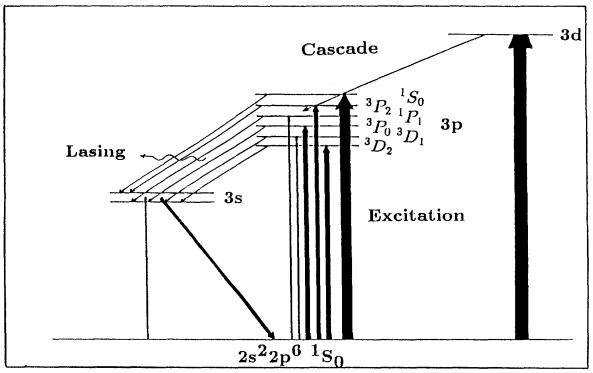

FIG. 2. Partial energy level diagram of neonlike Ar IX and collisional and radiative transitions.

This work was supported by the Deutsche Forschungsgemeinschaft, and one of us (D.O.C.) was supported by the DAAD. The authors acknowledge discussions with J. R. Roberts within the framework of a NATO collaborative research grant and thank H. R. Griem and R. C. Elton for comments.

[1] *X-Ray Lasers 1992, Proceedings of the 3rd International Colloqium on X-Ray Lasers,* edited by E. E. Fill, IOP Conf. Proc. No. 125 (Institute of Physics and Physical Society, London, 1992).

[2] R. C. Elton, *X-Ray Lasers* (Academic, New York, 1990).

[3] B. J. MacGowan, L. D. Da Silva, D. J. Fields, C. J. Keane, J. A. Koch, R. A. London, D. L. Matthews, S. Maxon, S. Mrowska, A. L. Osterheld, J. H. Scofield, G. Skimkaveg, J. E. Trebes, and R. S. Walling, Phys. Fluids B **4**, 2326 (1992).

[4] E. A. McLean, T. N. Lee, J. A. Stamper, C. K. Manka, and H. R. Griem, J. Opt. Soc. Am. B **9**, 350 (1992).

[5] D. L. Matthews, P. L. Hagelstein, M. D. Rosen, M. J. Eckart, M. N. Ceglio, A. Hazi, H. Medecki, B. J. MacGowan, J. E. Trebes, B. L. Whitten, E. M. Campbell, C. W. Hatcher, A. M. Hawryluk, R. L. Kauffman, D. L. Pleasance, G. Rambach, J. H. Scofield, G. Stone, and T. Weaver, Phys. Rev. Lett. **54**, 100 (1985).

[6] G. A. Doschek, U. Feldman, and A. K. Bhatia, Phys. Rev. A **43**, 2565 (1991).

[7] R. C. Elton, R. U. Datla, J. R. Roberts, and A. K. Bhatia, Phys. Rev. A **40**, 4142 (1989).

[8] R. C. Elton, R. U. Datla, J. R. Roberts, and A. K. Bhatia, Phys. Scr. **41**, 449 (1990).

[9] C. C. Chang, P. Greve, K.-H. Kolk, and H.-J. Kunze, Phys. Scr. **29**, 132 (1984).

[10] A. K. Bhatia, U. Feldman, and J. F. Seely, At. Data Nucl. Data Tables **32**, 435 (1985)

[11] H. Zhang, D. H. Sampson, R. E. Clark, and J. B. Mann, At. Data Nucl. Tables **37**, 17 (1987).

[12] M. Mohan, M. Le Dourneuf, and A. Hibber, J. Phys. B **24**, 299 (1991).

[13] M. Klapisch, Comput. Phys. Commun. **2**, 239 (1971).

[14] M. Klapisch, J. L. Schwob, B. S. Fraenkel, and J. Oreg, J. Opt. Soc. Am. **61**, 148 (1977).

[15] A. Bar-Shalom, M. Klapisch, and J. Oreg, Phys. Rev. A **38**, 1773 (1988).

[16] A. L. Osterheld, B. K. F. Young, R. S. Walling, W. H. Goldstein, J. H. Scofield, M. Chen, G. Shimkaveg, M. Carter, R. Shepherd, B. J. MacGowan, L. Da Silva, D. Matthews, S. Maxon, R. London, and R. E. Stewart, in *X-Ray Lasers 1992* (Ref. [1]), p. 309.

[17] M. H. Chen and K. J. Reed, Phys. Rev. A **40**, 2292 (1989).